Propeller Performance Prediction in an Artificially Generated Wake Field Using RANSE

João Baltazar*, Bart Schuiling†, and Douwe Rijpkema†
*IST Universidade de Lisboa, Portugal, †MARIN, Wageningen/the Netherlands
joao.baltazar@tecnico.ulisboa.pt

1 Introduction

Marine propellers usually operate behind a ship and are subject to a non-uniform inflow field due to the ship's boundary layer and wake system. This flow field is responsible for unsteady loads on the blades and often for the occurrence of unsteady cavitation phenomena, which are important in the analysis of shaft vibrations and pressure fluctuations.

RANSE (Reynolds-Averaged Navier-Stokes Equations) solvers are becoming a widely used tool for the modelling of the unsteady flow around propellers operating behind a ship. However, RANSE solvers are also associated with large computational requirements. Mikkelsen et al. (2007) introduced a method using body-forces for the generation of the ship wake field. These body-forces were combined with RANSE for the prediction of the propeller performance without the presence of the ship hull, reducing substantially the computational cost. A similar method was implemented by Shin et al. (2011) for unsteady cavitation simulations. These results have shown the feasibility of the method for the generation of a desired ship hull wake and prediction of the blade-load variations.

The aim of the present paper is to present a method for an accurate prediction of the propeller unsteady performance in an artificial wake field using RANSE in a cost-effective way. The propeller performance predictions in this artificial wake field are compared to the predictions in behind the ship. The paper is organised as follows: the major features of the numerical method are presented in Section 2; the test case and numerical set-up are described in Section 3; the numerical results are shown in Section 4; in Section 5 the main conclusions are drawn.

2 Numerical method

For the flow simulations, the RANSE (continuity and momentum equations) are solved using the ReFRESCO code (www.refresco.org). For turbulence closure, the $k-\omega$ SST turbulence model is chosen, Menter et al. (2003). A finite-volume discretisation technique with cell-centred collocated variables is used for solving the equations, and a pressure-correction equation based on the SIMPLE algorithm is used to ensure mass conservation. Time integration is performed implicitly with a second-order backward scheme. At each implicit time step, the non-linear system for velocity and pressure is linearised with Picard's method and a segregated approach is adopted for the solution of all transport equations. For the convective flux terms, a second-order scheme (QUICK) is applied for the momentum equations, and a first-order upwind scheme is applied for the turbulence model equations.

Body-forces are added to the momentum equation to generate the wake field. Based on the Rankine-Froude momentum theory and considering a uniform inflow velocity along the x direction, in this case equal to the ship velocity V_S, the local body-force $F_{x,y,z}$ on the actuator disc for an intended wake field $V_{w_{x,y,z}}$ may be written as

$$\begin{aligned} F_x &= -1/2\rho\,(V_S - V_{w_x})\,(V_S + V_{w_x})\,\frac{\Delta A}{\Delta V} \\ F_y &= 1/2\rho\,(V_S + V_{w_x})\,V_{w_y}\,\frac{\Delta A}{\Delta V} \\ F_z &= 1/2\rho\,(V_S + V_{w_x})\,V_{w_z}\,\frac{\Delta A}{\Delta V} \end{aligned} \quad , \tag{1}$$

where ΔA is the cell area perpendicular to the axial direction and ΔV is the cell volume. We note that the minus sign represents the deceleration of the flow in the x direction, simulating the bare hull wake field.

Due to the strong interaction between the axial and the transversal flows, the body-forces are calibrated iteratively by adjusting the wake velocity components:

$$\begin{aligned} F_x^{(i)} &= -1/2\rho\left(V_S - V_{w_x}^{(i)}\right)\left(V_S + V_{w_x}^{(i)}\right)\frac{1}{\Delta V^{1/3}} \\ F_y^{(i)} &= 1/2\rho\left(V_S + V_{w_x}^{(0)}\right)V_{w_y}^{(i)}\frac{1}{\Delta V^{1/3}} \qquad , \; i = 1, 2, \ldots, \\ F_z^{(i)} &= 1/2\rho\left(V_S + V_{w_x}^{(0)}\right)V_{w_z}^{(i)}\frac{1}{\Delta V^{1/3}} \end{aligned} \tag{2}$$

with

$$V_{w_{x,y,z}}^{(i)} = V_{w_{x,y,z}}^{(0)} - \beta\left(V_{w_{x,y,z}}^{(i-1)} - V_{w_{x,y,z}}^{(0)}\right), \tag{3}$$

where the cell area and volume are assumed proportional to h^2 and h^3 respectively, with h as the typical cell size, $V_{w_{x,y,z}}^{(0)}$ represents the intended wake field and β is a relaxation factor assumed equal to 0.5. In the present work, the body-forces are applied one propeller diameter upstream of the propeller plane.

3 Test case and numerical set-up

The KRISO Container Ship (KCS) is considered in the present study. For this ship there is an extensive experimental data set available, which has been used in the comparisons with contemporary CFD codes used in hydrodynamics, see for instance, Larsson et al. (2014). The KCS is a single screw container ship built only as a model with a scale ratio of 31.5994. It has a length between prependiculars of $L_{pp} = 7.2786$m, with a draft of 0.3418m and wetted surface of 9.4379m^2. It was equipped with a five blade right-handed propeller with a diameter of 0.25m. The propeller has a mean pitch-diameter ratio of 0.95, a blade-area ratio of 0.8 and a skew angle of 24 degrees at the tip.

The simulation of the viscous flow around KCS with operating propeller behind is first considered. The calculation is carried out with fixed free-surface, at a ship speed of 2.196m/s and an imposed propeller rotation rate of 9.75rpm. The corresponding Reynolds and Froude numbers based on the length between perpendiculars are 1.4×10^7 and 0.26, respectively. A rectangular computational domain is considered. The size of the computational domain is $3L_{pp}$ at upstream, $6L_{pp}$ at downstream, and $4L_{pp}$ in both transverse and vertical directions. At the propeller region, a sliding block is defined to implement the effect of propeller rotation. The total length and radius of the propeller domain are $0.325D$ and $0.55D$, respectively, where D is the propeller diameter. The inlet is located at $0.15D$ in front of the propeller plane and the outlet is at $0.175D$ behind it. For the generation of the grids, the grid meshing tool HEXPRESS (www.numeca.com), which uses an unstructured grid approach with hanging nodes for refinement, is considered for the hull domain. For the propeller domain, a multi-block structured grid is generated using the grid meshing package GridPro (www.gridpro.com). The grid sizes are 18.4M and 2.9M cells for the hull domain and the propeller domain, respectively. For the prediction of the nominal wake field, a bare hull simulation with the same fixed free-surface is made. A similar grid in comparison with the KCS with operating propeller is generated, keeping the computational domain dimensions. In this case the grid size is 18.8M cells. A comparison of the grids used in the simulations around the KCS with and without propeller is shown in Fig. 1.

For the simulation of the nominal wake field, an iterative calibration of the body-forces is made. Calculations are carried out without the propeller geometry (hub only) in a cylindrical domain with a length of $5D$ in all directions. The grid is generated using the grid meshing tool HEXPRESS and consists in 3.2M cells. For the prediction of the propeller performance in behind conditions using the artificial generated wake field, a similar computational domain is defined. In this case, the propeller region is defined as a separate sliding block, and the same propeller grid as used in the KCS calculations with operating propeller is considered. A comparison of the grids used in the simulations with and without propeller, here referred as open-water conditions, is shown in Fig. 2.

In this study, a fine boundary layer resolution is applied for all grids to obtain $y^+ \sim 1$. The boundary conditions remained fixed for all calculations: no-slip and impermeability conditions are applied at the propeller, hub and hull; at the inlet the ship velocity, an turbulence intensity of 1% and an eddy-viscosity

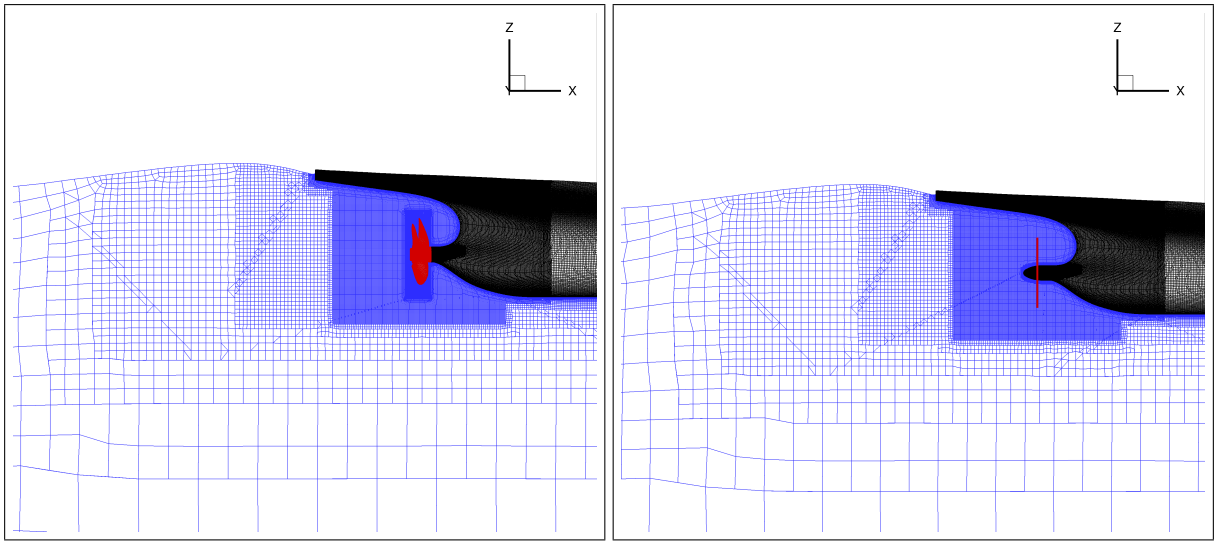

Fig. 1: Overview of the grids for the propeller simulations in behind condition (left) and bare hull simulations (right). The red line in the right figure represents the wake field extraction location.

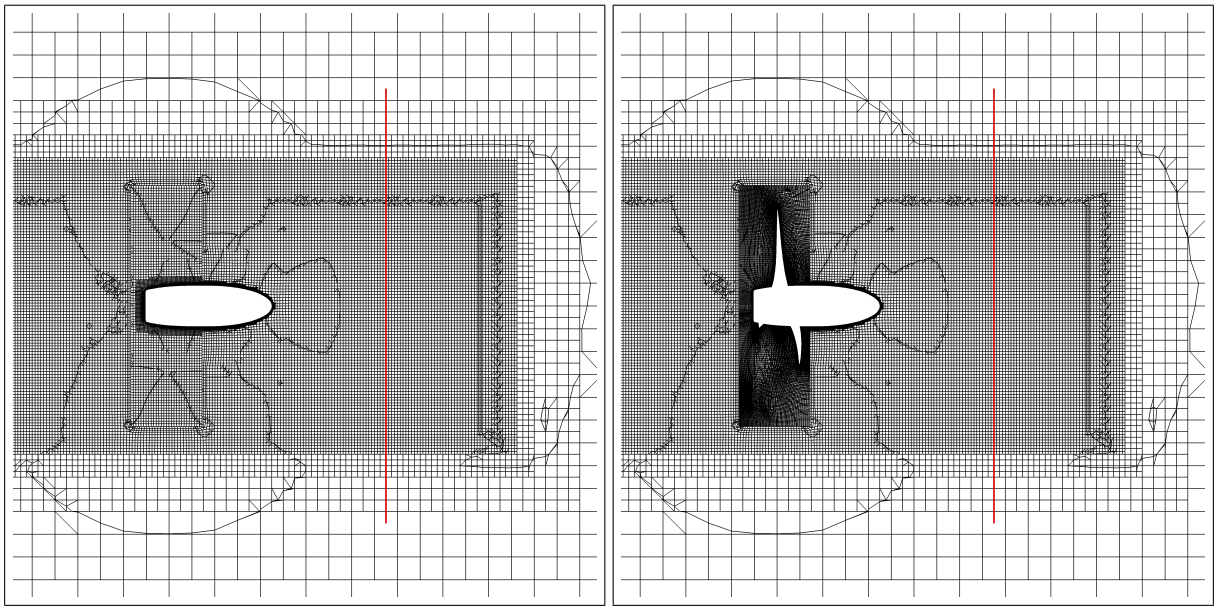

Fig. 2: Overview of the grids for the generation of the wake field (left) and propeller simulations without hull (right). The red line represents the body-forces location.

ratio of $\mu_t/\mu = 1$ are prescribed; for the open-water outlet boundary, a zero downstream gradient is assumed for all flow variables; for the hull free-surface and side boundaries zero normal derivatives are applied to the velocity and to the turbulence quantities, whereas the normal velocity is set equal to zero; finally, a constant pressure equal to the undisturbed flow pressure is considered for the hull outlet and bottom boundaries, and the open-water outer boundary.

4 Results

Results are presented and analysed for the four RANSE simulations in this section. The propeller operating conditions are defined by a single non-dimensional parameter: the advance coefficient $J = V_S/(nD)$, where $n = \Omega/(2\pi)$ is the rate of revolution. The general performance characteristics of the propeller are defined by the thrust coefficient $K_T = T/(\rho n^2 D^4)$, and the torque coefficient $K_Q = Q/(\rho n^2 D^5)$, where T is the thrust, Q the torque and ρ the fluid density.

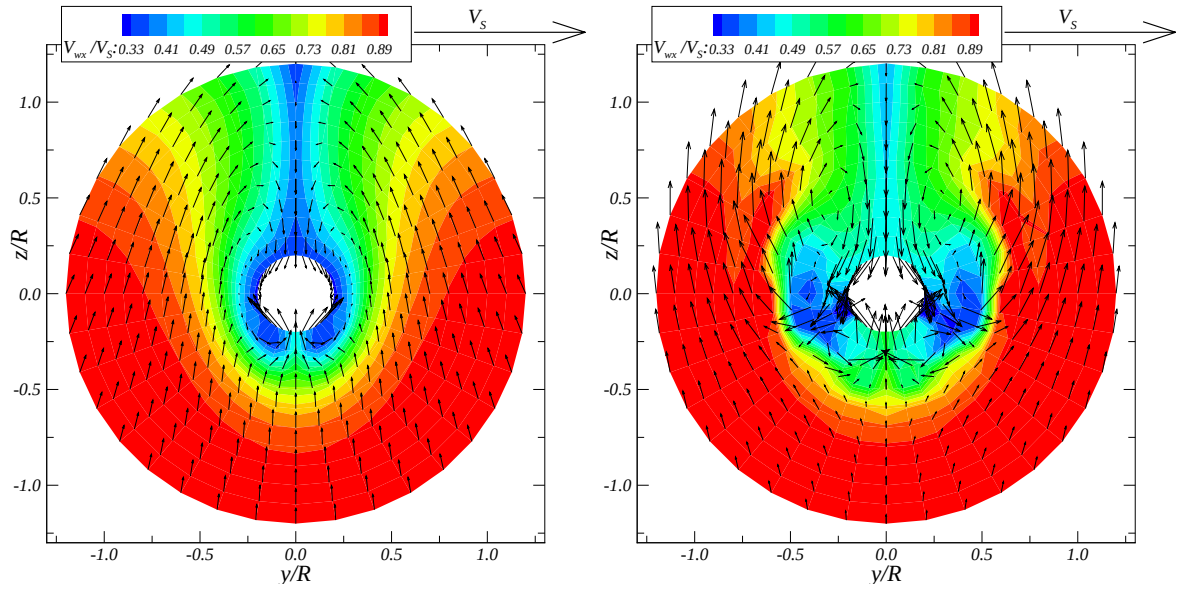

Fig. 3: Predicted nominal wake field from bare hull simulation (left) and generated wake field using calibrated body-forces (right). R denotes the propeller radius.

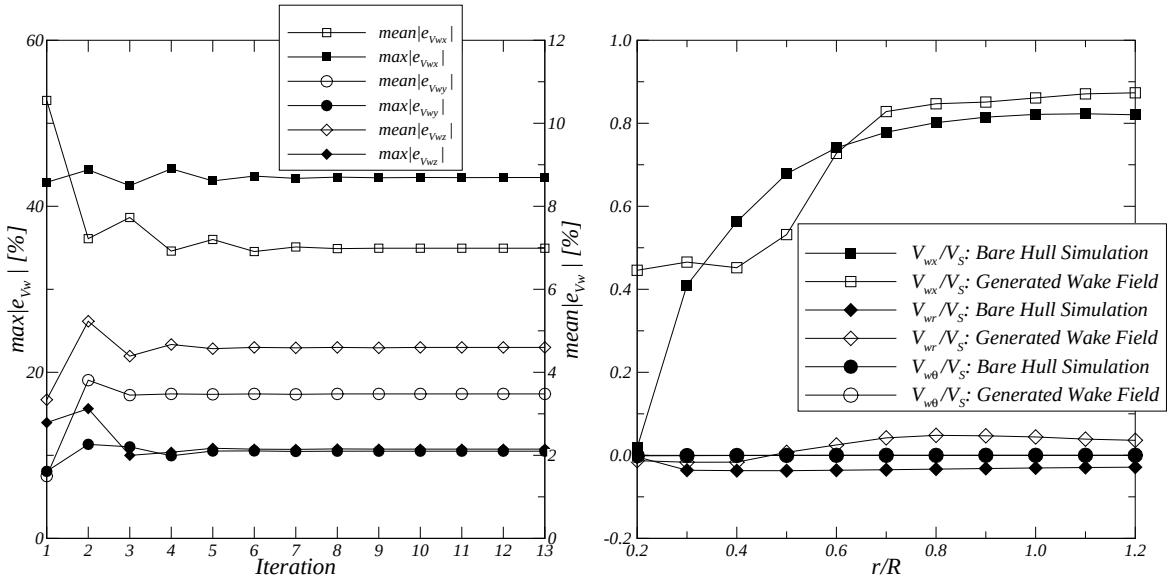

Fig. 4: Convergence history of the mean and maximum differences between the generated wake field using body-forces and the predicted nominal wake field in respect to the ship velocity (left). Comparison of the circumferential average wake fields (right).

4.1 Wake field generation

From the bare hull simulation, the nominal wake field is obtained. The wake velocities are extracted from discrete points in the propeller plane with an angular resolution of 10 degrees at 11 radial sections. For the iterative solution of the transport equations, maximum normalised residuals around 10^{-1} and 10^{-4} are obtained for the velocities and pressure, respectively. The predicted nominal wake field is presented in Fig. 3-(left), where a wake peak is observed near the 12 o'clock position (corresponding to azimuthal position of 0 degrees). From the open-water simulations without propeller, an artificial wake field is generated using iteratively calibrated body-forces. The obtained wake field is shown in Fig. 3-(right). In this case, iterative convergence below 10^{-6} is obtained for all flow quantities. From the comparison with the nominal wake field, a weaker peak is predicted and larger transversal velocities are observed at the inner radii. Note that these two cases correspond to steady computations.

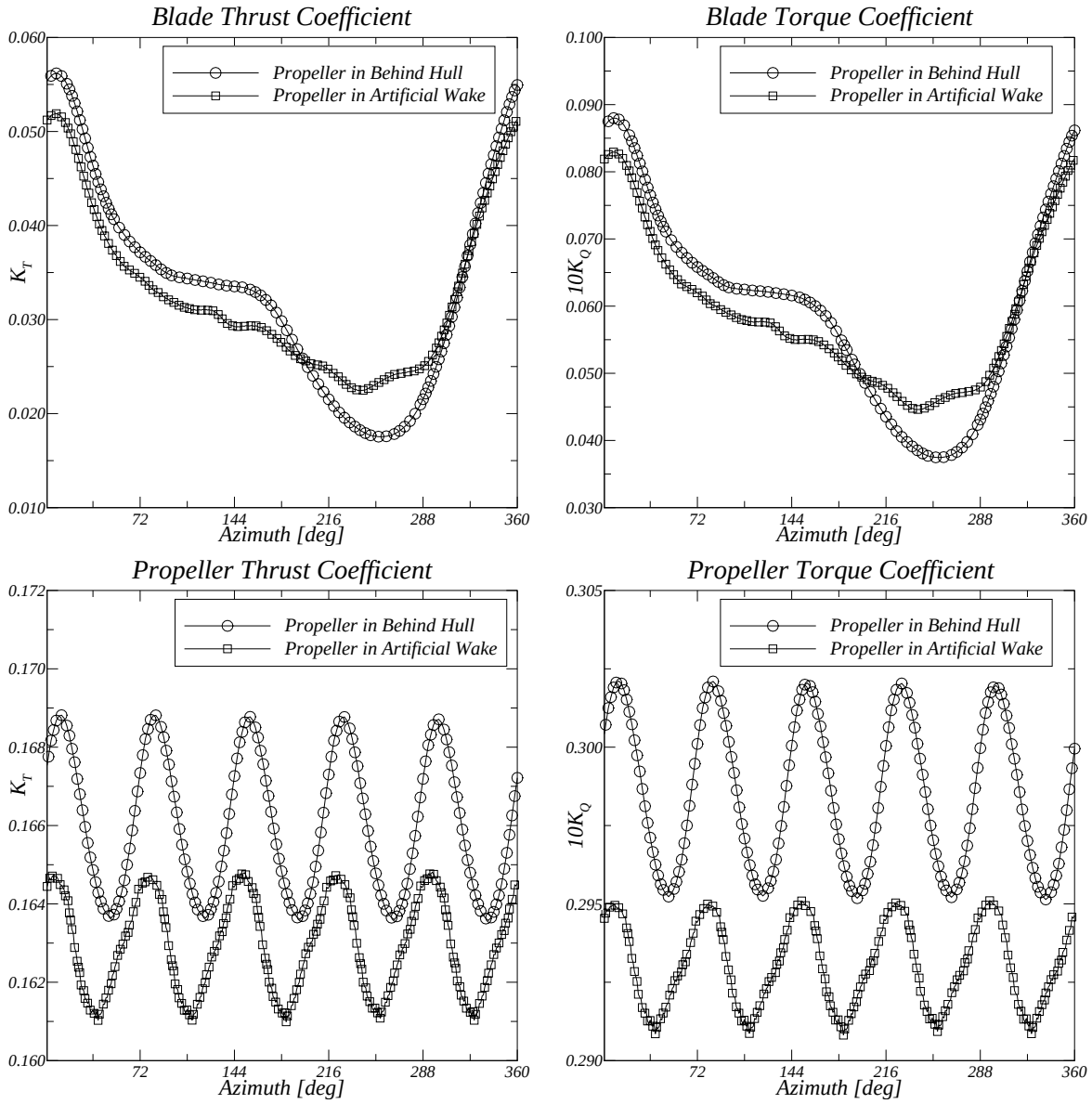

Fig. 5: Thrust (left) and torque (right) fluctuations for a single blade (top) and the propeller (bottom) during one revolution.

The convergence history of the mean and maximum differences between the generated wake field using body-forces and the predicted nominal wake field, in respect to the ship velocity, is presented in Fig. 4-(left). Stagnation of the mean and maximum differences is obtained after 8 iterations. Mean differences of 7% are obtained for the axial velocity. The transversal velocities present lower mean differences in the range of $3-5\%$. For the maximum differences, large values are obtained at the inner radii near the azimuthal positions of 110 and 250 degrees. The axial velocity present a maximum difference around 43%, whereas for the transversal velocities the maximum differences are of the order of 10%. The comparison of the cylindrical components for the circumferential average wake fields is shown in Fig. 4-(right). Significant differences at the inner radii are observed between the axial components.

4.2 Propeller in behind condition

The unsteady simulations of the KCS propeller operating behind hull and in an artificially generated wake field are presented and the performance predictions compared. For the propeller simulations operating in behind hull condition, the time step is tuned to obtain an angular step of 2 degrees. In this calculations, average and maximum Courant numbers around 0.78 and 106 are obtained, respectively. For the iterative

Table 1: Mean, first and second harmonic amplitudes of the blade frequency for the total thrust and torque coefficients.

	Behind Hull		Artificial Wake	
n	$K_T^{(n)}$	$10K_Q^{(n)}$	$K_T^{(n)}$	$10K_Q^{(n)}$
0	0.1660	0.2985	0.1630	0.2930
1	0.0025	0.0034	0.0017	0.0019
2	0.0002	0.0002	0.0002	0.0003

solution, 50 iterations are considered for each time step, leading to a maximum normalised residual around 10^{-1} for the velocitites and pressure. For the propeller simulations in the artificially generated wake field, an angular step of 1 degree is considered. The corresponding time step led to the average and maximum Courant numbers around 0.88 and 33, respectively. In this case, 100 iterations are considered for the iterative solution of the transport equations, where a maximum normalised residual below 10^{-2} is obtained for the velocities and pressure.

Figure 5 shows the thrust and torque fluctuations for a single blade and the propeller during one revolution. For the single blade force coefficients, the comparison shows that the thrust and torque fluctuations due to the wake peak are well captured by the computations in the artificial wake. In this case, the largest differences are observed near the azimuthal position of 252 degrees. Differences are also visible in the propeller thrust and torque coefficients. The mean $K_{T,Q}^{(0)}$, first $K_{T,Q}^{(1)}$ and second harmonic $K_{T,Q}^{(2)}$ amplitudes of the blade frequency for the total thrust and torque coefficients are presented in Table 1. The definitions are:

$$K_{T,Q}(\theta) = K_{T,Q}^{(0)} + K_{T,Q}^{(1)} \sin\left(K\theta + \phi^{(1)}\right) + K_{T,Q}^{(2)} \sin\left(2K\theta + \phi^{(2)}\right), \tag{4}$$

where θ is the azimuthal position, K the number of propeller blades and $\phi^{(1,2)}$ the phase angles. The comparison shows that lower mean and first harmonic amplitudes are obtained in the propeller simulations with the artificial generated wake. Negligible values are obtained for the second harmonic amplitude. The relative differences for the mean total thrust and torque coefficients are equal to -1.8%.

5 Conclusion

A method for the prediction of the propeller unsteady performance in a artificially generated wake field using body-forces is presented. This method offers an alternative to the full RANS approach. The two approaches are compared and the main reasons for the differences in the propeller performance prediction are attributed to the artificially generated wake field used in the propeller computations without hull. In this work, the nominal wake field obtained from the bare hull simulation is considered, which may contribute for the under-prediction of the thrust and torque, since the interaction between the propeller and the nominal wake field is neglected. In addition, the artificial wake field generated from iteratively calibrated body-forces present differences higher than 10% in respect to the ship velocity at the inner radii. These differences are attributed to the strong interaction between the axial and transversal wake flows. Alternative boundary conditions combined with body-forces will be considered for future work to improve the replication of the nominal wake field. Nevertheless, minor differences in the order of 1.8% are obtained for the mean propeller thrust and torque coefficients between the two approaches.

References

L. Larsson, F. Stern, M. Visonneau (eds.) (2014). *Numerical Ship Hydrodynamics: An Assessment of the Gothenburg 2010 Workshop*. Springer.

F.R. Menter, M. Kuntz, and R. Langtry (2003). Ten years of industrial experience with the SST turbulence model. *Proceedings of the Fourth International Symposium on Turbulence, Heat and Mass Transfer*, **4**, 625–632.

R. Mikkelsen, P. Andersen, J.N. Sorensen (2007). Modeling of behind condition wake flow in RANS computation on a conventional and high skew propeller. 10th Numerical Towing Tank Symposium, Hamburg, Germany.

K.W. Shin, P. Andersen, R. Mikkelsen (2011). Cavitation simulation on conventional and highly-skewed propellers in the behind-hull condition. Second International Symposium on Marine Propulsors, smp'11, Hamburg, Germany.